biomedicines

MDPI

Article

Post-Surgical Depositions of Blood Products Are No Major Confounder for the Diagnostic and Prognostic Performance of CEST MRI in Patients with Glioma

Nikolaus von Knebel Doeberitz [1,*], Florian Kroh [2,3], Laila König [4], Philip S. Boyd [2], Svenja Graß [1], Cora Bauspieß [1], Moritz Scherer [5], Andreas Unterberg [5,6], Martin Bendszus [6,7], Wolfgang Wick [6,8], Peter Bachert [2,3], Jürgen Debus [4,6,9], Mark E. Ladd [2,3,6], Heinz-Peter Schlemmer [1,6], Steffen Goerke [2], Andreas Korzowski [2] and Daniel Paech [1,10,*]

1 Division of Radiology, German Cancer Research Center (DKFZ), 69120 Heidelberg, Germany
2 Division of Medical Physics in Radiology, German Cancer Research Center (DKFZ), 69120 Heidelberg, Germany
3 Department of Physics and Astronomy, University of Heidelberg, 69120 Heidelberg, Germany
4 Department of Radiation Oncology, Heidelberg University Hospital, 69120 Heidelberg, Germany
5 Department of Neurosurgery, University Hospital Heidelberg, 69120 Heidelberg, Germany
6 Faculty of Medicine, University of Heidelberg, 69120 Heidelberg, Germany
7 Department of Neuroradiology, University Hospital Heidelberg, 69120 Heidelberg, Germany
8 Department of Neurology, University Hospital Heidelberg, 69120 Heidelberg, Germany
9 Clinical Cooperation Unit Radiation Oncology, German Cancer Research Center (DKFZ), 69120 Heidelberg, Germany
10 Department of Neuroradiology, University Hospital Bonn, 53127 Bonn, Germany
* Correspondence: n.knebel@dkfz.de (N.v.K.D.); d.paech@dkfz.de (D.P.)

Abstract: Amide proton transfer (APT) and semi-solid magnetization transfer (ssMT) imaging can predict clinical outcomes in patients with glioma. However, the treatment of brain tumors is accompanied by the deposition of blood products within the tumor area in most cases. For this reason, the objective was to assess whether the diagnostic interpretation of the APT and ssMT is affected by methemoglobin (mHb) and hemosiderin (Hs) depositions at the first follow-up MRI 4 to 6 weeks after the completion of radiotherapy. A total of 34 participants underwent APT and ssMT imaging by applying reconstruction methods described by Zhou et al. ($APTw_{asym}$), Goerke et al. ($MTR_{Rex}APT$ and $MTR_{Rex}MT$) and Mehrabian et al. (MT_{const}). Contrast-enhancing tumor (CE), whole tumor (WT), mHb and Hs were segmented on contrast-enhanced T_1w_{CE}, T_2w-FLAIR, T_1w and T_2*w images. ROC-analysis, Kaplan–Meier analysis and the log rank test were used to test for the association of mean contrast values with therapy response and overall survival (OS) before (WT and CE) and after correcting tumor volumes for mHb and Hs (CE_C and WT_C). CE_C showed higher associations of the $MTR_{Rex}MT$ with therapy response (CE: AUC = 0.677, p = 0.081; CE_C: AUC = 0.705, p = 0.044) and of the $APTw_{asym}$ with OS (CE: HR = 2.634, p = 0.040; CE_C: HR = 2.240, p = 0.095). In contrast, WT_C showed a lower association of the $APTw_{asym}$ with survival (WT: HR = 2.304, p = 0.0849; WT_C: HR = 2.990, p = 0.020). Overall, a sophisticated correction for blood products did not substantially influence the clinical performance of APT and ssMT imaging in patients with glioma early after radiotherapy.

Keywords: chemical exchange saturation transfer MRI; amide proton transfer; semi-solid magnetization transfer; glioma; radiotherapy; therapy response; overall survival; blood; correction; hemosiderin; methemoglobin

check for updates

Citation: von Knebel Doeberitz, N.; Kroh, F.; König, L.; Boyd, P.S.; Graß, S.; Bauspieß, C.; Scherer, M.; Unterberg, A.; Bendszus, M.; Wick, W.; et al. Post-Surgical Depositions of Blood Products Are No Major Confounder for the Diagnostic and Prognostic Performance of CEST MRI in Patients with Glioma. *Biomedicines* **2023**, *11*, 2348. https://doi.org/10.3390/biomedicines11092348

Academic Editor: Fengchao Lang

Received: 13 July 2023
Revised: 11 August 2023
Accepted: 16 August 2023
Published: 23 August 2023

1. Introduction

Standard of care for diffuse glioma includes maximum safe resection, with subsequent radio- and chemotherapy [1]. Yet, since treatment-related changes, such as pseudoprogression and radionecrosis have similar morphological imaging features compared to

progressing glioma tissue, therapy response assessment and survival prediction are well-known challenges in clinical neuro-oncology, with possibly harmful consequences for the patient [2]. In this regard, the promising clinical potential of functional MR imaging methods, including perfusion-weighted imaging, MR spectroscopy and chemical exchange saturation transfer (CEST) imaging has been shown in recent years [3,4]. Imaging of the amide-proton transfer (APT) and of the semi-solid magnetization transfer (ssMT) relies on the selective radio frequency (RF) saturation of protons bound in peptide bindings or sub-cellular macromolecules, with subsequent magnetization transfer to bulk water through chemical exchange or spin–spin couplings, respectively [5] (collectively referred to as CEST imaging in the following). Several groups have demonstrated that APT and ssMT imaging could predict the therapy response and survival of patients with glioma before and after radiochemotherapy [6–10]. Others have demonstrated that imaging of the APT and ssMT could also be used to differentiate radiation-induced changes from tumor progression as early as the first follow-up after the completion of radiotherapy [11–17]. However, treatment of brain tumors is frequently accompanied by perioperative and radiation-induced disruptions of the blood–brain-barrier with subsequent depositions of blood products, such as methemoglobin (mHb) and hemosiderin (Hs), in the tumor area [18]. mHb and Hs are both proteinaceous, contain paramagnetic iron (Fe^{3+}) and exist to varying degrees as conglomerates of insoluble macromolecules. For this reason, mHb and Hs not only have a strong influential impact on T_1 and T_2, but should also contribute to the APT and ssMT pool. However, whilst several groups have demonstrated that CEST imaging of the APT can differentiate between acute and subacute stages of intracranial hemorrhage [19–21], little is known about the influence of mHb and Hs on the clinical performance of APT and ssMT imaging in patients with glioma in the post-radiotherapy interval. Furthermore, CEST contrasts are heavily dependent on the metrics used for their reconstruction form the Z-spectrum [7,22,23]. Therefore, the purpose of this study was to assess the relevance of advanced correction methods for mHb and Hs depositions in the tumor area for the clinical performance of APT and ssMT contrasts under the application of different reconstructions methods first described by Zhou et al. ($APTw_{asym}$) [24], Goerke et al. (MTR_{Rex}APT and MTR_{Rex}MT) [25] and Mehrabian et al. (MT_{const}) [7].

2. Materials and Methods

Eligible for this prospective clinical study were all patients who received radiotherapy for diffuse glioma at the Department of Radiation-Oncology of the University Hospital Heidelberg between September 2018 and December 2021, and who were 18 years of age or older, had a Karnofsky Performance Score of at least 50 and had the legal capacity to consent. Eventually, 72 study participants (61 with initial disease and 11 with relapsing/progressive disease) were enrolled and received CEST imaging at the first follow-up MRI 4 to 6 weeks after the completion of radiotherapy. Two participants had to be excluded from the analysis due to heavy motion artifacts, seven due to incomplete datasets and one for excessive perioperative ischemia. The data cut-off was 3 May 2022. The association of CEST imaging with therapy response and progression-free survival (PFS), as well as with overall survival (OS), was previously investigated in two studies involving 61 and 49 participants of the same cohort, respectively [5,10]. Therapy response was assessed based on longitudinal clinical data and MRI according to the revised response assessment in neuro oncology (RANO) criteria by two radiologists with 6 (N.v.K.D.) and 11 (D.P.) years of experience in neuroimaging at the time of data acquisition [26]. The results of the assessment were reconciled with institutional multidisciplinary tumor board decisions to account for potential changes in relevant medications, such as antiangiogenic or cytotoxic drugs, and changes in clinical status. Overall survival (OS) was assessed by written request to the relevant public registries and was available for 54 of 62 evaluable participants. Due to differences in the tumor biology between midline gliomas and hemispherical gliomas, the data of five study participants with midline gliomas were additionally excluded from the analysis [27,28]. Finally, given that the associations of the investigated contrasts with therapy response and

survival are influenced by the presence of residual contrast enhancement on MRI [6,11], the data of 34 participants with available survival data, hemispherical gliomas and residual contrast enhancement were analyzed (Figure 1).

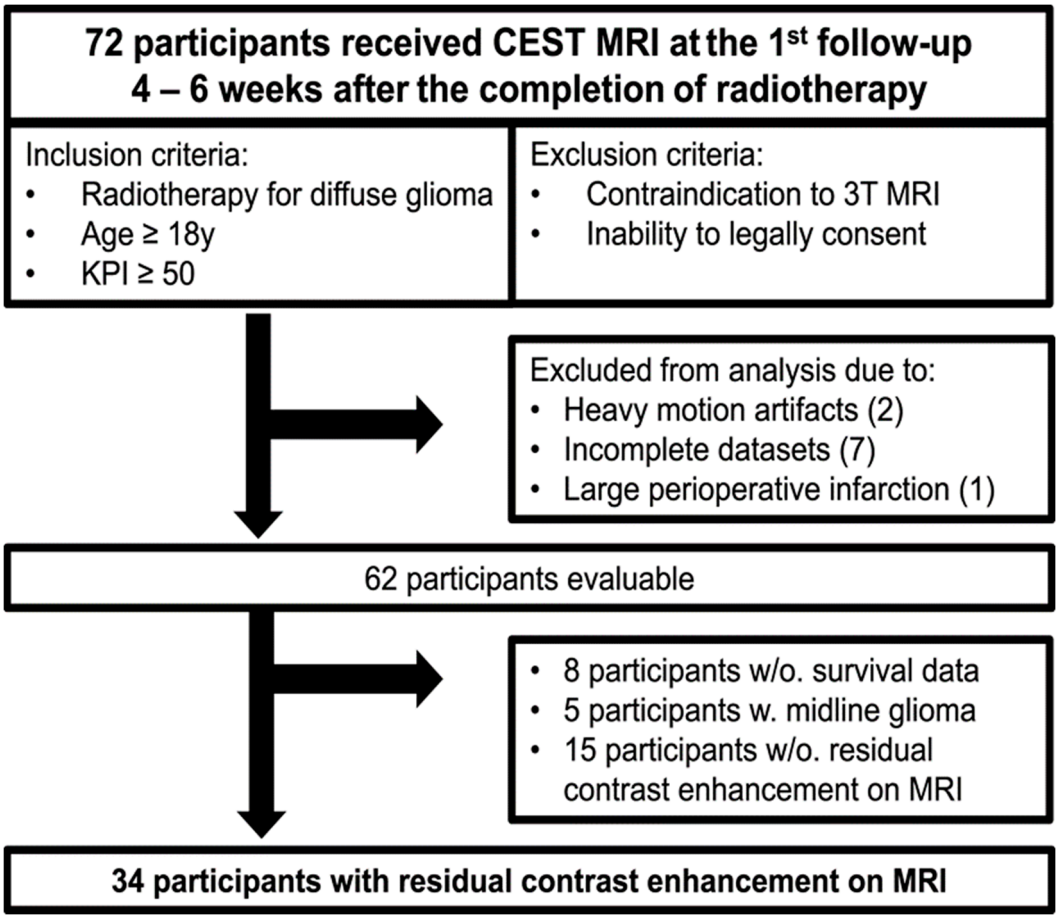

Figure 1. Flowchart. Displayed is a description of the whole study cohort participants and the 34 participants that were eventually included in the analysis. Between September 2018 and December 2021, 72 participants with diffuse glioma received CEST imaging 4 to 6 weeks after the completion of radiotherapy. In total, 11 participants had to be excluded from the analysis due to the indicated reasons. Given that diffuse midline gliomas are biologically distinct from hemispherical gliomas [27,28] and previous studies observed a dependency of CEST contrasts on the presence of residual tumor-associated contrast enhancement on MRI [6,11], the datasets of 34 participants with hemispherical gliomas, presence of residual contrast enhancement on MRI and available survival data were included in the analysis. The associations of mean CEST contrast values with therapy response and overall survival were tested by Kaplan–Meier analyses and log rank tests. KPI = Karnofsky Performance Score; w. = with; w/o. = without.

Histology: For all of the 34 study participants evaluated, tumor tissue was available for histopathological analysis after biopsy or surgical resection. Routinely, *IDH*-, *ATRX*-, LOH1p19q- and *MGMT*-status were assessed, and histopathological classification was performed in accordance with the 2016 version of the World Health Organization (WHO)'s criteria for the classification of primary central nervous system (CNS) tumors. Please see Table 1 for a detailed description of the histopathological tumor characteristics for all evaluated participants.

Table 1. Clinical characteristics. Displays a summary of the most relevant clinical characteristics for all 34 evaluated study participants with glioma.

Characteristic		Number (n)	Percentage
Age at diagnosis	Mean 59.2 ± 15.6	34	
Therapy response at the 1st FU [1]	Stable disease (SD)	16	47.1%
	Progressive disease (PD)	18	52.9%
Overall survival	Median 287 days (min. 63, max. 1271)		
Alive at data cut-off		10	29.4%
Sex	Male	19	55.9%
	Female	15	44.1%
Treatment for	Initial disease	31	91.2%
	Progressive disease	3	8.8%
Therapy	Radiation	6	17.6%
	Chemoradiation	28	82.4%
	Debulking surgery	21	61.8%
Diagnosis	GBM [2]	28	82.4%
	Gliosarcoma	2	5.9%
	Astrocytoma	4	11.8%
WHO [3]	II	1	2.9%
	III	1	2.9%
	IV	32	94.1%
IDH [4] status	*IDH*wt [5]	28	82.4%
	*IDH*mut [6]	4	11.8%
	n/a	2	5.9%
MGMT promotor methylation	Yes	19	55.9%
	No	12	35.3%
	n/a	3	8.8%

[1] FU = follow-up MRI; [2] GBM = glioblastoma, [3] WHO II–IV = World Health Organization classification system for primary brain tumors grade II–IV; [4] *IDH* = isocitrate-dehydrogenase isotype 1/2; [5] wt = wildtype; [6] mut = mutation.

Image Acquisition and Postprocessing: Image acquisition was performed on a 3T whole-body MR scanner (MAGNETOM Prisma; Siemens Healthineers, Erlangen, Germany) with an integrated transmit body coil and a 64-channel head/neck receiving coil. The CEST data were processed in Matlab® (Mathworks, version 2019b, Natick, MA, USA) using customized scripts.

Imaging of the APT and ssMT according to Goerke et al. (MTR_{Rex}APT and MTR_{Rex}MT): A 3D spiral-centrally reordered gradient-echo acquisition sequence (snapshot CEST [29,30]) was applied with the same image readout parameters (matrix = 128 × 104 × 16, resolution = 1.7 × 1.7 × 3 mm^3) and presaturation as previously described by Goerke et al. [25]. For presaturation, trains of 148 Gaussian-shaped radio frequency (RF) pulses (echo time (TE) = 2.75 ms, repetition time (TR) = 5.5. ms, flip angle = 7°, puls length (tp) = 0.02 s and duty cycle = 80%) with two amplitudes (B_1 = flip angle/(γ·tp)) of 0.6 µT and 0.9 µT were acquired at 57 unequally distributed offsets in the range between ±250 ppm and −300 ppm for normalization at two M_0, resulting in a saturation time of 3.7 s and a total measurement time of 7:34 min. The WASABI [31] (3:41 min) approach was applied to yield B_0 and B_1 maps, using the same image readout and similar presaturation parameters as described above. In this case, presaturation was performed by sampling 31 equally distributed frequency offsets around ±2 ppm. For post-processing, the CEST and WASABI data were first co-registered with a rigid registration algorithm in MITK (version v2022.10). Then, the CEST data were processed in Matlab® (Mathworks, version 2019b, Natick, MA, USA). A correction of B_0 inhomogeneities was achieved by shifting the Z-spectra along $\Delta\omega$ [32] and denoising was achieved under the application of a principle component-based algorithm [32]. The reconstruction of the MTR_{Rex}APT and MTR_{Rex}MT from the Z-spectrum was performed as described in [25] under the application of a four-pool Lorentzian-fit ±250 ppm up- and down-field of the water offset (0 ppm: direct water saturation, 3.5 ppm: APT, −3.5 ppm: rNOE, and −2.5 ppm: ssMT) with $MTR_{Rex} = \frac{1}{Z} - \frac{1}{Z_{ref}}$ (Z = all fitted

pools, Z_{ref} = fitted pools—pool of interest). A two-point "contrast-correction" method first proposed by Windschuh et al. [33] was applied for additional B_1-correction.

Imaging of the ssMT according to Mehrabian et al. (MT_{const}): Image readout parameters, presaturation, co-registration of CEST data and B_0 correction were the same as described above. The MT_{const} was reconstructed from the Z-spectrum of the CEST data with B_1 = 0.6 µT with a Lorentzian fit around ±6 ppm with [7]:

$$S(\Delta) = 1 - \left(MT + \sum_{i=1}^{4} \frac{A_i}{1 + \left(\frac{\Delta - \Delta_{0i}}{0.5 w_i} \right)^2} \right)$$

$$[A_i, \Delta_{0i}, w_i] = [\text{amplitude}, \text{centrefrequency}, \text{width}] \quad (1)$$

Imaging of the APT according to Zhou et al. ($APTw_{asym}$): Again, pulse sequence and image readout parameters were the same as described above [24]. In accordance with recent consensus guidelines [23], four rectangular RF pulses with a B_1 of 2 µT (t_{sat} = 0.2 s and 95% duty cycles) at 16 frequency offsets at ±4 (1), ±3.75 (2), ±3.5 (2), ±3.25 (2), and ±3 (1) ppm and an additional M_0 at −300 ppm were obtained, resulting in a scan time of 2:00 min. Co-registration of the CEST data and B_0-correction of the Z-spectra was performed under the application of similar post-processing methods as described above with APTw = Z(−3.5 ppm) − Z(3.5 ppm).

Quantitative T_1 mapping: The longitudinal relaxation time of water (T_1) was measured via quantitative mapping with the same image readout parameters as above. A saturation recovery sequence with recovery times (t_{rec}) of 0.1, 0.25, 0.5, 1.0, 1.5, 2.0, 2.5, 3.5, 5.0, 7.5 and 10.0 s and $M_z(t_{rec}) = M_0 + (M_z(0) - M_0) \cdot e^{-t_{rec}/T_1}$ [25] was applied, resulting in a scan time of 1:15 min.

Segmentation of tumor volumes and blood products: Three-dimensional segmentations of tumor volumes and blood products were also performed in Matlab® (Mathworks, version 2019b, Natick, MA, USA). mHb (detectable in 14 cases) was defined as hyperintense material on T_1w, and Hs (detectable in 33 cases) as dark tissue on T_2*w susceptibility-weighted imaging (SWI). Contrast-enhancing (CE) and whole tumor volumes (WT) were segmented on contrast-enhanced T_1w ($T1w_{CE}$) and T_2w fluid-attenuated inversion recovery (T_2w-FLAIR) images. WT encompassed CE plus adjacent T_2w-FLAIR-hyperintense signal alterations. Larger mHB depositions that were identifiable as such on T_1w_{CE} and T_2w-FLAIR (e.g., due to localization in the resection cavity or associated T_2w-FLAIR signal drops that indicated surrounding Hs (Figure 2b)) were grossly excluded (Figure S1). Contrast-enhancing and whole tumor volumes corrected for mHb and Hs (CE_C and WT_C) were calculated from CE and WT in Matlab® by subtracting the overlapping mHb and Hs volumes (Figure A1).

Statistical analyses: Mann–Whitney-U-test was applied to test for differences between the mean CEST contrast values of blood products and corrected tumor volumes, as well as between uncorrected and corrected tumor volumes. Receiver operating characteristic (ROC) analyses were performed to test for the association of mean CEST contrast values of uncorrected and corrected tumor volumes with therapy response, as assessed according to the RANO criteria. Kaplan–Meier analyses and log rank tests were used to test for the association of mean CEST contrast values of uncorrected and corrected tumor volumes with OS. In-house software in Matlab® (Mathworks, version 2019b, Natick, MA, USA) was used for all statistical analyses. $p \leq 0.05$ was considered as being statistical significant.

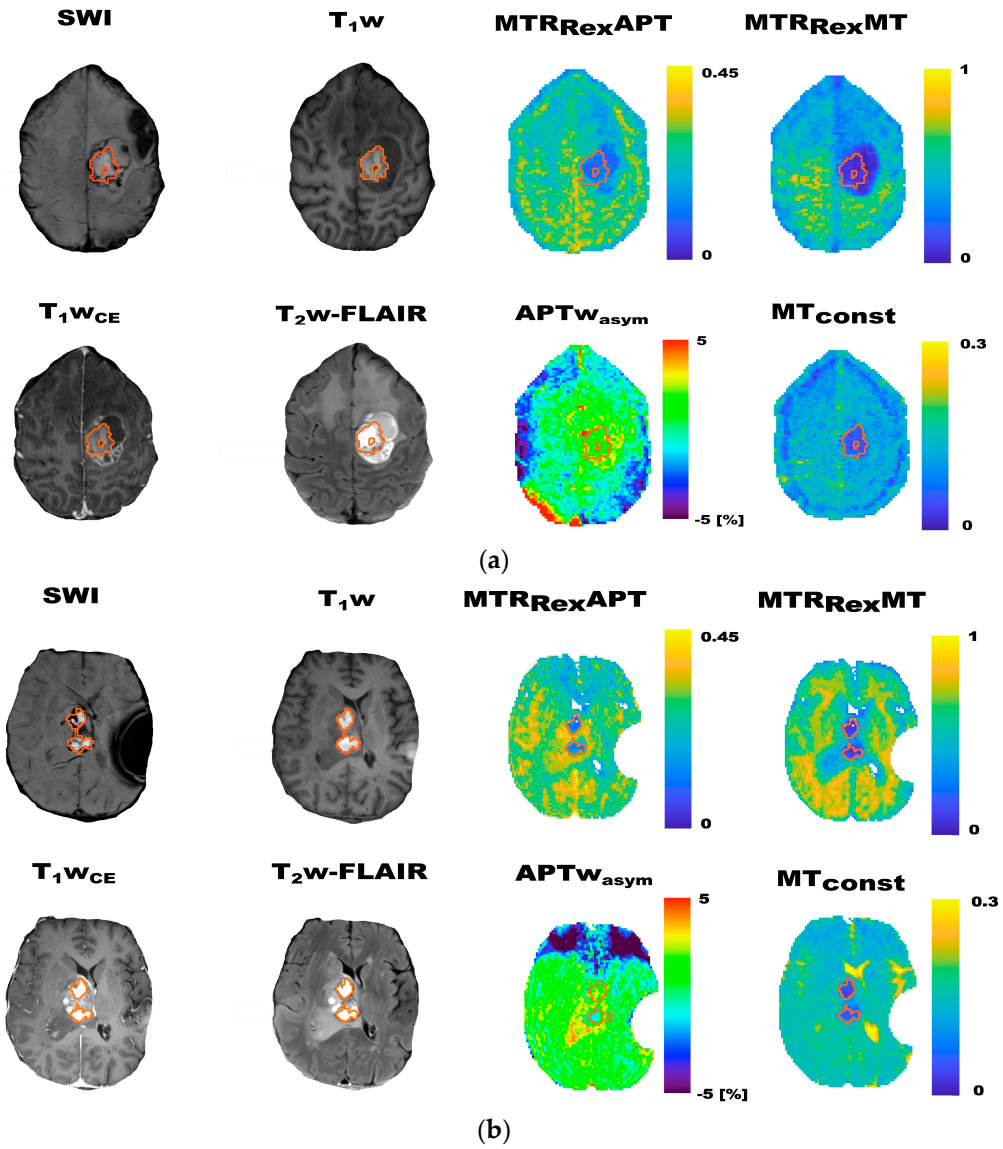

Figure 2. Exemplary contrast maps of two participants with larger methemoglobin depositions (mHb) in the tumor area (**a**,**b**). Given are T_2* susceptibility-weighted (SWI), T_1w, contrast-enhanced T_1w (T_1w_{CE}) and T_2w-FLAIR images, as well as CEST contrast maps of $MTR_{Rex}APT$, $MTR_{Rex}MT$, $APTw_{asym}$ and MT_{const} imaging. The ROIs indicate the T_1w-hyperintese mHb on all contrast maps. mHb visually showed markedly decreased values pronounced on $MTR_{Rex}APT$, $MTR_{Rex}MT$ and MT_{const} contrast maps. The figure highlights the visible depression of the investigated CEST contrasts in correspondence to larger mHb depositions.

3. Results

In total, 72 study participants (mean age 59 ± 16 years; 43 male) underwent CEST MRI at the first follow-up 4 to 6 weeks after the completion of radiotherapy. The data of 34 participants (19 male, 15 female; mean age of 59.2 ± 15.6 years) with diffuse hemispherical glioma who had available data on therapy response and survival, and showed residual contrast enhancement on MRI were included in the analysis. A total of 16 participants were assessed as having stable disease (SD) and 18 were assessed as having progressive disease (PD). Median OS was 287 days (min. 63 and max. 1271 days), with 24/34 participants having reached an endpoint by the data cut-off on 3 May 2022. Detailed clinical characteristics of the analyzed study cohort are provided in Table 1.

3.1. CEST Contrast Maps of Participants with Larger Depositions of mHb and Hs

Exemplary contrast maps of four study participants with larger depositions of mHb (2) and Hs (2) in the tumor area are displayed in Figures 2 and 3, respectively. Associated quantitative T_1 maps are depicted in Figure A2. Visually, larger depositions of Hs showed remarkably higher values on the $MTR_{Rex}APT$ contrast maps sharply confined to the drawn ROIs (Figure 3). This was not observed on the other contrast maps. Furthermore, larger mHb depositions visually showed remarkably dropped values on $MTR_{Rex}APT$, $MTR_{Rex}MT$, MT_{const} and T_1 (Figures 2 and A2) contrast maps, which was recapitulated by lower $MTR_{Rex}APT$, $MTR_{Rex}MT$ and MT_{const} mean values of mHb in comparison to CE_C and WT_C (Table A1). Exemplary fitted Z-spectra for representative voxels of contrast-enhancing tumor tissue, peritumoral T_2w-FLAIR-hyperintense signal alterations, and mHb and Hs in an exemplary participant with larger depositions of mHb and Hs are shown in Figures S1–S4.

3.2. Differences between the Mean CEST Contrast Values of Uncorrected and Corrected Tumor Volumes

Even though there were differences between the mean $MTR_{Rex}APT$, $MTR_{Rex}MT$ and MT_{const} contrast values of mHb and CE_C/WT_C, as well as the mean $MTR_{Rex}MT$ and $APTw_{asym}$ contrast values of Hs and CE_C/WT_C (Table A1), there were no differences between the mean values of any contrast for uncorrected and corrected tumor volumes (Figure 4). The mean $MTR_{Rex}APT$ values were 0.249 ± 0.036 vs. 0.247 ± 0.037 ($p = 0.854$) for CE vs. CE_C, and 0.243 ± 0.029 vs. 0.243 ± 0.029 (0.990) for WT vs. WT_C, respectively. For the $MTR_{Rex}MT$ the mean contrast values were 0.376 ± 0.071 vs. 0.381 ± 0.073 ($p = 0.695$) for CE vs. CE_C, and 0.464 ± 0.065 vs. 0.470 ± 0.063 ($p = 0.615$) for WT vs. WT_C, respectively. For the $APTw_{asym}$ the mean contrast values were 1.388 ± 0.563% vs. 1.379 ± 0.553% ($p = 0.893$) for CE vs. CE_C, and 0.914 ± 0.536 vs. 0.898 ± 0.528% ($p = 0.759$), respectively. The mean contrast values of the MT_{const} for CE vs. CE_C were 0.171 ± 0.029 vs. 0.173 ± 0.028 ($p = 0.704$), and those for WT vs. WT_C were 0.162 ± 0.023 vs. 0.163 ± 0.023 ($p = 0.023$).

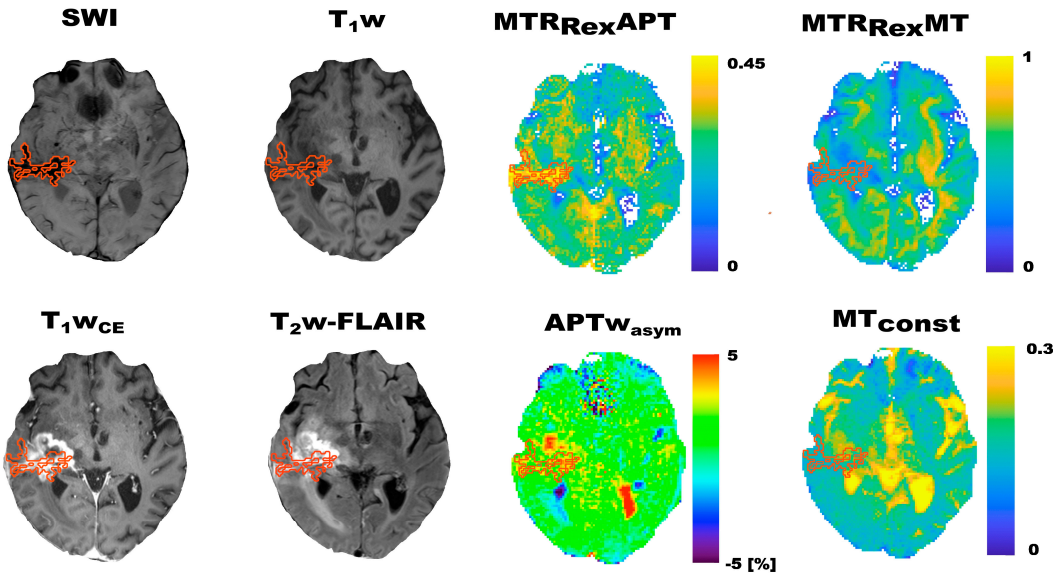

(**a**)

Figure 3. *Cont.*

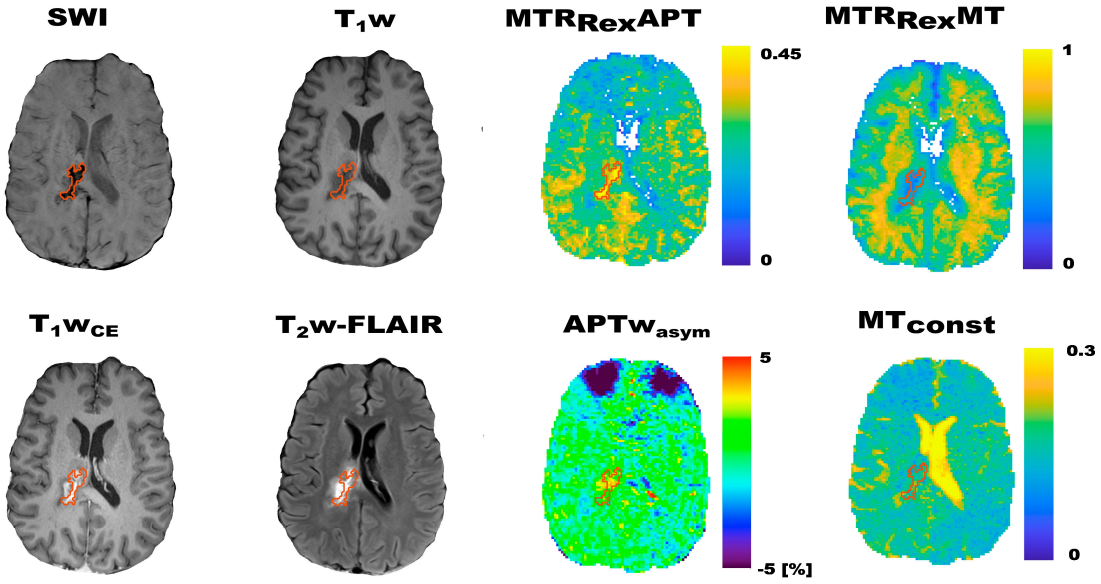

Figure 3. Exemplary contrast maps of two participants with larger hemosiderin depositions (Hs) in the tumor area (**a**,**b**). Given are T_2* susceptibility-weighted (SWI), T_1w, contrast-enhanced T_1w (T_1w_{CE}) and T_2w-FLAIR images, as well as CEST contrast maps of $MTR_{Rex}APT$, $MTR_{Rex}MT$, $APTw_{asym}$ and MT_{const} imaging. The ROIs indicate Hs (dark on SWI) on all contrast maps. The $MTR_{Rex}APT$ visually showed markedly elevated contrast values corresponding sharply to Hs in these participants. The figure highlights the visible increase, especially of the $MTR_{Rex}APT$ in correspondence to larger Hs depositions.

3.3. Association of CEST Contrast Values of Uncorrected and Corrected Tumor Volumes with Therapy Response

In the ROC analyses, the $MTR_{Rex}MT$ was the only contrast that showed a noticeable improvement regarding the association of the mean contrast values of tumor tissue with therapy response at the first follow-up. The area under the curve (AUC) for differentiating participants with PD and SD according to the mean contrast values (with PD > SD) was 0.677 ($p = 0.081$) for CE and 0.705 ($p = 0.044$) for CE_C. However, there were no differences in AUCs for WT (AUC = 0.635, $p = 0.184$) and WT_C (AUC = 0.628, $p = 0.184$). The association of MT_{const} mean contrast values with therapy response of uncorrected and corrected tumor volumes did not show relevant differences (CE: AUC = 0.826, $p = 0.001$; CE_C: AUC = 0.816, $p = 0.002$; WT: AUC = 0.868, $p < 0.001$; WT_C: AUC = 0.861, $p < 0.001$). The $MTR_{Rex}APT$ (CE: AUC = 0.438, $p = 0.546$; CE_C: AUC = 0.424, $p = 0.458$; WT: AUC = 0.566, $p = 0.523$; WT_C: 0.569, $p = 0.501$) and $APTw_{asym}$ (CE: AUC = 0.514, $p = 0.904$; CE_C: AUC = 0.504, $p = 0.986$; WT: AUC = 0.538, $p = 0.717$; WT_C: AUC = 0.552, $p = 0.617$) mean contrast values did not show any association with therapy response before and after the correction. The ROC curves for the investigated CEST contrasts are displayed in Figure 5. The results of the ROC analysis are summarized in Table A2.

3.4. Association of Mean CEST Contrast Values of Uncorrected and Corrected Tumor Volumes with Overall Survival

In the Kaplan–Meier analyses, the $APTw_{asym}$ mean contrast values showed a slightly lower association with survival for CE_C (CE: HR = 2.634, $p = 0.040$; CE_C: HR = 2.634, $p = 0.040$) and a slightly higher association with survival for WT_C (WT: HR = 2.304, $p = 0.084$; WT_C: HR = 2.990, $p = 0.020$), compared to the respective uncorrected tumor volumes, with a shorter OS of participants with higher mean values compared to the cohort median (CE: 215 vs. 392 days; CE_C 215 vs. 392 days; WT: 225 vs. 392 days; WT_C 215 vs. 392 days). The $MTR_{Rex}APT$ mean values also showed a lower association with survival for CE_C (CE:

HR = 2.439, p = 0.056, OS = 225 vs. 416 days; CE_C: HR = 2.110, p = 0.110, OS = 253 vs. 392 days), whilst for whole tumor volumes, no association with survival could be observed regardless of the correction (WT: HR = 1.526, p = 0.417, OS = 225 vs. 392 days; WT_C: HR = 1.525, p = 0.417, OS = 225 vs. 392). For the MT_{const}, the correction had no measurable impact on its trend towards an association with survival for contrast-enhancing tumor volumes (CE: HR = 2.330, p = 0.068, OS = 228 vs. 315 days; CE_C: HR = 2.330, p = 0.068, OS = 228 vs. 315 days) and on its association with survival for whole tumor volumes (WT: HR = 2.536, p = 0.044, OS = 215 vs. 392 days; WT_C: HR = 2.535, p = 0.044, OS = 215 vs. 392 days). The $MTR_{Rex}MT$ was not associated with survival regardless of the correction (CE: HR = 0.958, p = 0.919, OS = 315 vs. 280 days; CE_C: HR = 1.068, p = 0.964, OS = 315 vs. 280 days; WT: HR = 1.389, p = 0.559, OS = 294 vs. 280 days; WT_C: HR = 1.179, p = 0.847, OS = 315 vs. 225 days). The Kaplan–Meier plots are depicted in Figure 6 and the results are summarized in Table A3.

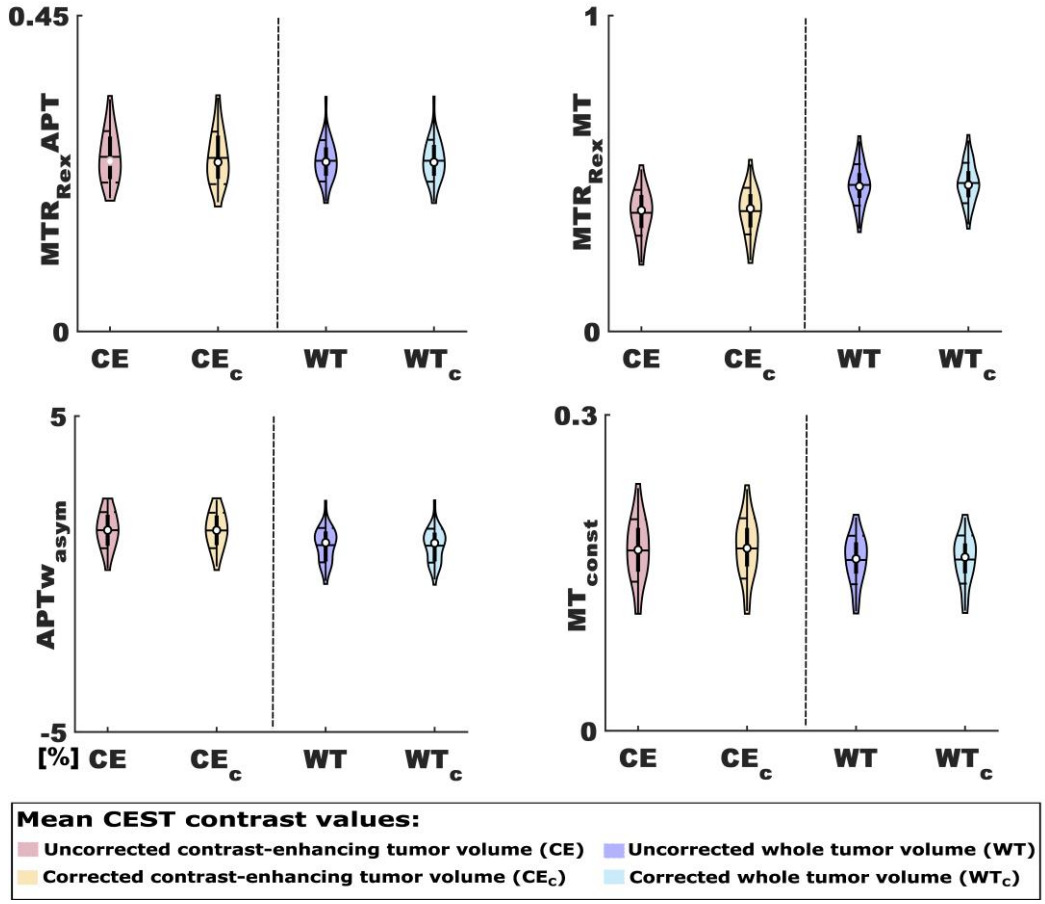

Figure 4. Mean CEST contrast values of uncorrected and corrected tumor volumes. Given are violin plots for $MTR_{Rex}APT$, $MTR_{Rex}MT$, $APTw_{asym}$ and MT_{const} mean contrast values for contrast-enhancing and whole tumor volumes without (CE and WT) and with (CE_C and WT_C) correction for mHb and Hs. The figure highlights that there were no relevant differences between the CEST contrast values of tumor volumes that were uncorrected and corrected for methemoglobin (mHb) and hemosiderin (Hs) depositions.

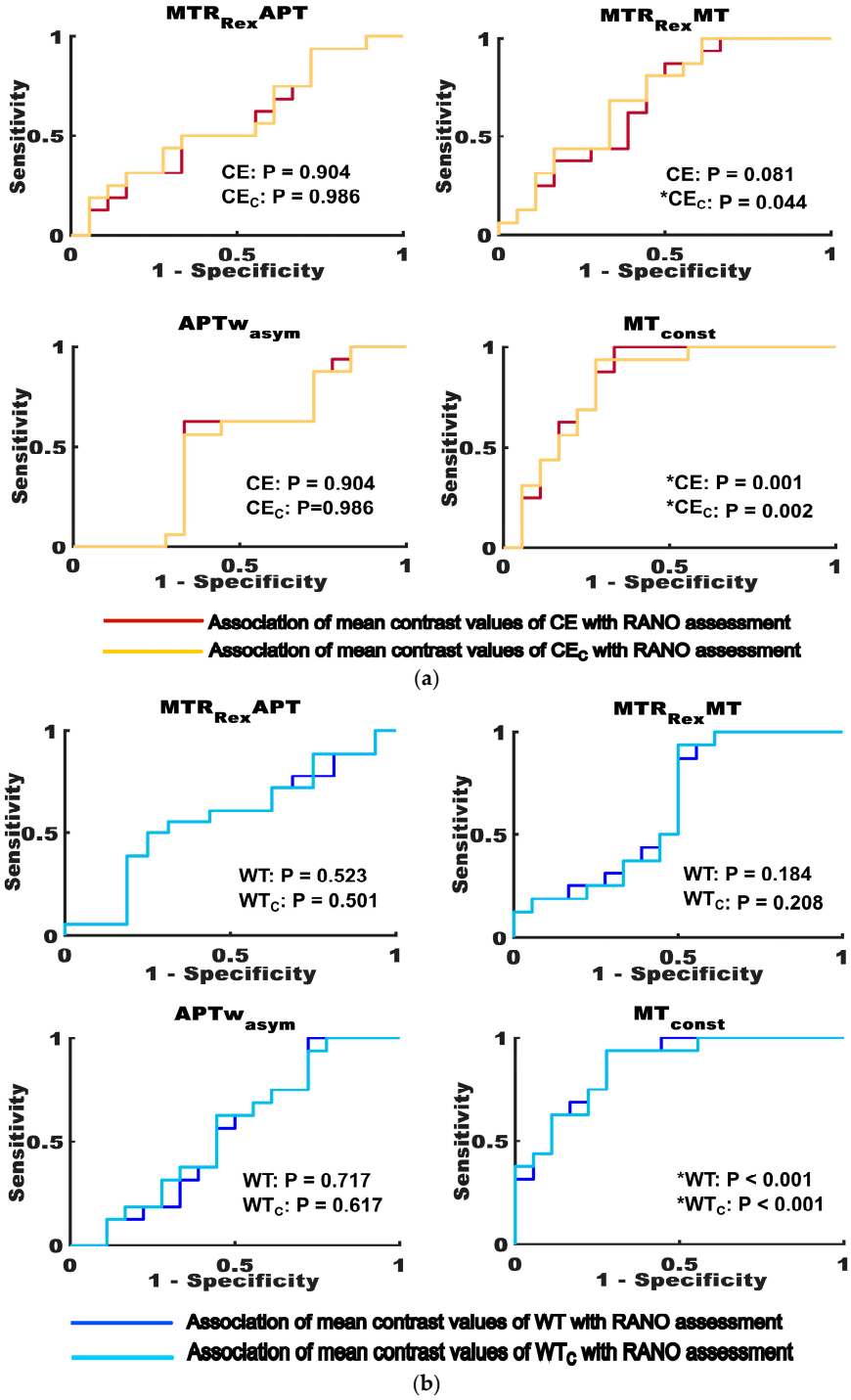

Figure 5. Association of mean CEST contrast values for uncorrected and corrected tumor volumes with therapy response. The figure shows the receiver operating characteristic (ROC) curves testing for the ability of $MTR_{Rex}APT$, $MTR_{Rex}MT$, $APTw_{asym}$ and MT_{const} mean contrast values to differentiate between participants with progressive disease (higher mean values compared to the cohort median) and stable disease (lower mean values), as assessed according to the response assessment in neuro-oncology (RANO) criteria. (**a**) shows the results for uncorrected (CE—dark red) and corrected (CE_C—yellow) contrast-enhancing tumor volumes. (**b**) shows the results for uncorrected (WT—dark blue) and corrected (WT_C—light blue) whole tumor volumes. Statistically significant results ($p \leq 0.05$) are indicated with an asterisk (*). The figure highlights that there were only marginal differences in the association of CEST contrast values with therapy response for uncorrected and corrected tumor volumes, which mainly affected the $MTR_{Rex}MT$.

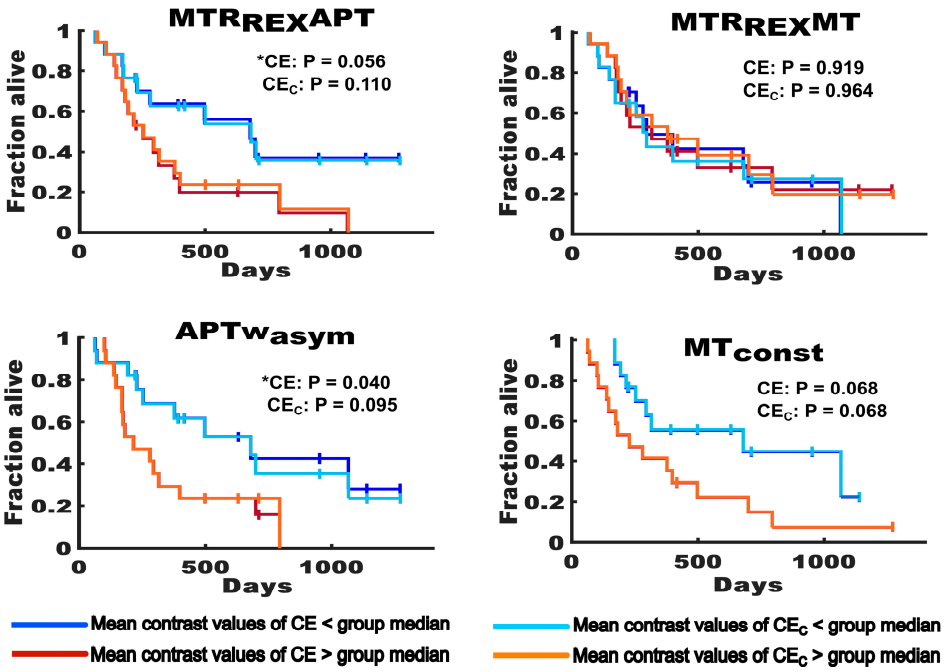

(**a**)

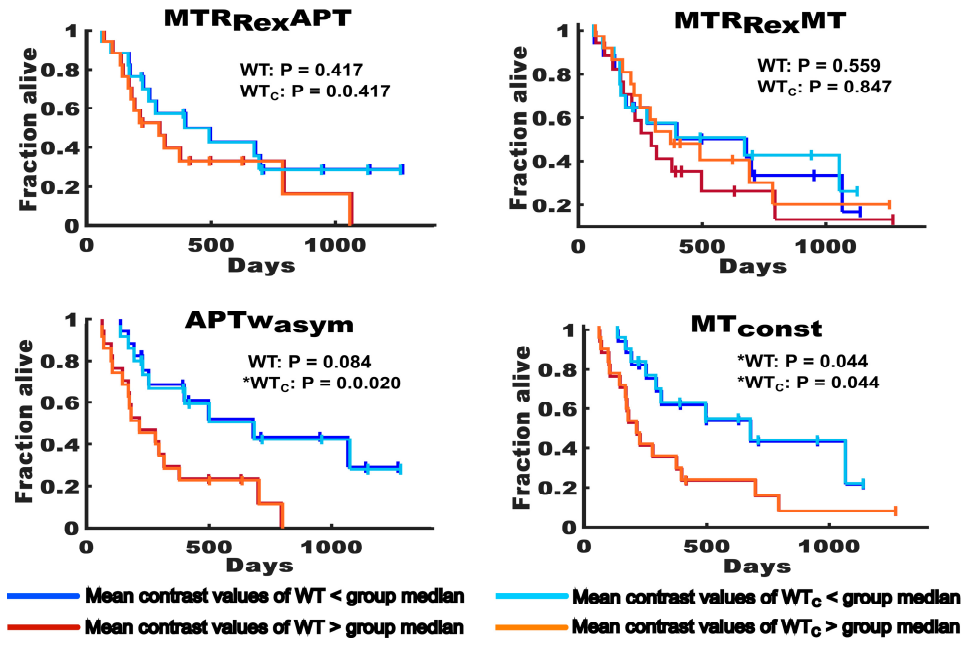

(**b**)

Figure 6. Association of the mean CEST contrast values for uncorrected and corrected tumor volumes with survival. The figure shows Kaplan–Meier plots displaying the association of $MTR_{Rex}APT$, $MTR_{Rex}MT$, $APTw_{asym}$ and MT_{const} mean contrast values of uncorrected (CE and WT) and corrected (CE_C and WT_C) tumor volumes with overall survival. (**a**) shows the plots for contrast-enhancing tumor volumes (CE and CE_C). (**b**) shows the plots for whole tumor volumes (WT and WT_C). The survival of participants with mean values below the group medians is indicated by dark blue graphs for uncorrected tumor volumes (CE and WT) and by turquoise graphs for corrected tumor volumes (CE_C and WT_C). The survival of participants with mean values above the group medians is indicated by brown graphs for uncorrected tumor volumes (CE and WT) and by orange graphs for corrected tumor volumes (CE_C and WT_C). Statistically significant results ($p \leq 0.05$) are indicated with an asterisk (*). The figure highlights that there were only marginal differences in the association of CEST contrast values with overall survival that mainly affected the $MTR_{Rex}APT$ and the $APTw_{asym}$.

3.5. Supermedian Analysis of the Mean CEST Contrast Values of Uncorrected and Corrected Tumor Volumes

To understand the impact of the blood product correction on the tumor-associated mean CEST contrast values in greater detail, we also assessed how many participants switched from the respective groups with higher mean CEST contrast values compared to the respective cohort medians (supermedian) to the groups with lower mean values (submedian) and vice versa upon correcting tumor volumes for mHb and Hs. We observed that for CE_C in comparison to CE, one participant switched from super- to submedian and one participant from sub- to supermedian for $MTR_{Rex}APT$, $MTR_{Rex}MT$ and $APTw_{asym}$. Additionally, for WT_C in comparison to WT one participant switched from super- to submedian and one participant from sub- to supermedian for $MTR_{Rex}MT$. However, for the MT_{const}, no participants switched from super- to sub- or sub- to supermedian upon correcting any tumor volume for blood products. The results of this analysis with corresponding tumor mean CEST contrast values for the assessed participants and respective cohort medians are summarized in Table S1.

4. Discussion

Whilst several groups demonstrated the potential of CEST imaging in the diagnostic follow-up after hemorrhagic stroke, little is known about the influence of post-therapeutic depositions of blood breakdown products on the clinical performance of APT and ssMT imaging in the early post-radiotherapy interval. For this reason, the purpose of this study was to assess the impact of advanced correction methods for mHb and Hs on the association of most commonly employed APT and ssMT contrasts with therapy response and OS at the first follow-up 4 to 6 weeks after the completion of radiotherapy at 3T. Even though, the $MTR_{Rex}APT$ contrast maps showed markedly elevated values in correspondence with Hs, and the $MTR_{Rex}APT$, $MTR_{Rex}MT$ and MT_{const} contrast maps showed noticeably dropped values in correspondence with mHb, no relevant differences in mean contrast values between uncorrected and corrected tumor volumes could be detected. However, for corrected contrast-enhancing tumor volumes, a slightly stronger association of the $MTR_{Rex}MT$ with therapy response was observed, whilst the $MTR_{Rex}APT$ showed a moderately weaker association with survival. Interestingly, the $APTw_{asym}$ showed contradicting trends, with a somewhat weaker association with survival for corrected contrast-enhancing tumor volumes, and a slightly stronger association with survival for corrected whole tumor volumes. Concurrently, the association of MT_{const} mean values with therapy response and survival were unaffected by the correction.

In previous studies, Sawaya et al., Wang et al. and Ma et al. observed that asymmetry-based APTw imaging showed markedly elevated contrast values in rat models and in patients with acute and subacute cerebral bleeding, which very likely corresponded to accumulations of deoxygenized hemoglobin and mHb [13,19,20,34–36]. Lai et al., on the other hand, observed significantly reduced contrast values in the subacute stage of cerebral hemorrhage in a preclinical study, using an apparent exchange-dependent relaxation compensated metric of the APT (APT_{AREX}) [21]. Contrary to these findings, to our knowledge, there are no available published results on the CEST contrast behaviors of Hs.

The findings of Lai et al. are mirrored by decreased $MTR_{Rex}APT$, $MTR_{Rex}MT$ and MT_{const} values for mHb in comparison to corrected tumor volumes, which were observed on this study (Figure 2). Given that mHb contains paramagnetic Fe^{3+}, the observed contrast patterns might at least in part be explained by residual T_1 contributions especially to the MT_{const}, but to a lesser extent also to the other investigated CEST contrasts [5–7,22,34]. Since magnetization transfer between protons and free water through chemical exchange is base-triggered, pH might be another factor that could influence particularly APT-weighted CEST contrasts [5,22]. The visibly increased values on $MTR_{Rex}APT$ contrast maps that corresponded to Hs, on the other hand, are harder to explain (Figure 2). Hs consists of intracellular accumulations of insoluble and partially digested ferritin, which should be associated with a rather acidotic intralysosomal milieu, T_1 contributions from paramagnetic

Fe^{3+} and fewer mobile amide protons due to the insoluble state of the proteinaceous compounds [34]. Taken together, further research is needed to understand the physicochemistry behind the observed CEST contrast patterns of mHb and Hs.

Despite these observations and considerations, no relevant differences in the investigated CEST contrast mean values could be observed between the uncorrected and corrected tumor volumes. Concurrently, the correction only had a very minor impact on the association of the $MTR_{Rex}MT$ with therapy response and of the $MT_{Rex}APT$ and $APTw_{asym}$ with survival in this relatively small clinical cohort of 34 participants. Even though the contribution of mHb and Hs depositions to the contrast behavior of uncorrected and corrected tumor volumes could not be quantified, it seems reasonable to speculate that their amount was simply too small over the whole cohort to produce relevant effects. This might implicate that whilst larger mHb and Hs depositions are very visible, especially on $MTR_{Rex}APT$ contrast maps, advanced correction methods for the evaluation of CEST contrasts in the post therapeutic setting in representative clinical cohorts of patients with glioma could be of secondary relevance.

The relatively small cohort size, the subjective determination of mHb and Hs on T_1w and T_2*w imaging, and the lack of corresponding histopathological data for the assessed blood products are the major limitations of this study. Even though histopathological confirmation of remaining blood products in the tumor area is impossible to obtain, future studies assessing the impact of mHb and Hs on the clinical performance of CEST imaging in the early post-therapeutic interval might benefit from larger sample sizes (e.g., in multicenter trials) and support from AI-based automated segmentation tools for the definition of specific blood products.

5. Conclusions

A sophisticated correction for methemoglobin and hemosiderin did not substantially alter the clinical performance of APT and ssMT imaging at the first follow-up 4 to 6 weeks after the completion of radiotherapy in 34 participants with glioma. Larger blood product depositions were visible on APT and ssMT contrast maps and had minor effects on the clinical performance of the $MTR_{Rex}MT$ regarding therapy response assessment, and on that of the $MTR_{Rex}APT$ and $APTw_{asym}$ regarding patient outcome prediction.

Supplementary Materials: The following supporting information can be downloaded at: https://www.mdpi.com/article/10.3390/biomedicines11092348/s1, Figure S1: Fitted Z-spectra of contrast-enhancing tumor tissue, Figure S2: Fitted Z-spectra of tumor-associated T_2w-FLAIR-hyperintense signal alterations, Figure S3: Fitted Z-spectra of tumor-associated hemosiderin, Figure S4: Fitted Z-spectra of tumor-associated methemoglobin, Table S1: Supermedian analysis of mean CEST contrast values for uncorrected and corrected tumor volumes.

Author Contributions: Conceptualization, N.v.K.D.; Methodology, N.v.K.D., F.K., P.S.B., P.B., S.G. (Steffen Goerke), A.K. and D.P.; Software, F.K. and S.G. (Steffen Goerke); Validation, N.v.K.D., D.P., F.K., P.S.B. and A.K.; Formal Analysis, N.v.K.D.; Investigation, N.v.K.D.; Resources, L.K., H.-P.S., M.E.L., J.D., M.B., W.W., M.S. and A.U.; Data Curation, N.v.K.D., S.G. (Svenja Graß) and C.B.; Writing—Original Draft Preparation, N.v.K.D.; Writing—Review and Editing, N.v.K.D., D.P., F.K., P.S.B., S.G. (Svenja Graß), C.B., M.S., A.U., M.B., W.W., P.B., J.D., M.E.L., H.-P.S., S.G. (Steffen Goerke) and A.K.; Visualization, N.v.K.D.; Supervision, N.v.K.D.; Project Administration, N.v.K.D., F.K., A.K. and D.P.; Funding Acquisition, D.P. and S.G. (Steffen Goerke). All authors have read and agreed to the published version of the manuscript.

Funding: This research was funded by a grant from the German Research Foundation (DFG), Grant No. 445704496.

Institutional Review Board Statement: This study was conducted in accordance with the Declaration of Helsinki, and approved by the Ethics Committee of the Medical Faculty of the University of Heidelberg (protocol code: S-251/2018; date of approval: 7 June 2018).

Informed Consent Statement: Informed consent was obtained from all subjects involved in the study.

Data Availability Statement: Data generated or analyzed during the study are available from the corresponding author upon reasonable request.

Acknowledgments: We would like to thank all study nurses and radiographers who have enabled this research for their careful work. Namely, these are Jessica Engelhart, Vanessa Peregovic, Jennifer Reimold, Heike Streib-Retzbach, Regula Gnirs, Cora Weyrich, Marek Wolski, Marina Schuricht, Anne-Mareike Rau, Susanne Metzner and Sina Kammer.

Conflicts of Interest: The authors declare no conflict of interest.

Appendix A

Table A1. Mean CEST contrast values for methemoglobin, hemosiderin as well as uncorrected and corrected tumor volumes.

		mHb	**Hs**	**mHb**	**CE_C**	**mHb**	**WT_C**	**Hs**	**CE_C**	**Hs**	**WT_C**
$MTR_{rex}APT$	Mean	0.206	0.249	0.206	0.247	0.206	0.243	0.249	0.247	0.249	0.243
	SD	0.070	0.038	0.070	0.037	0.070	0.029	0.038	0.037	0.038	0.029
	P	0.035 *		0.042		0.052 *		0.817		0.568	
$MTR_{rex}MT$	Mean	0.272	0.325	0.272	0.381	0.272	0.470	0.325	0.381	0.325	0.470
	SD	0.098	0.074	0.098	0.073	0.098	0.063	0.074	0.073	0.074	0.063
	P	0.134		<0.001 *		<0.001 *		0.004 *		<0.001 *	
$APTw_{asym}$	Mean [%]	0.712	1.164	0.712	1.379	0.712	0.898	1.164	1.379	1.164	0.898
	SD [%]	1.595	0.837	1.595	0.553	1.595	0.528	0.837	0.553	0.837	0.528
	P	0.436		0.200		0.313		0.527		0.013 *	
MT_{const}	Mean	0.145	0.163	0.145	0.173	0.145	0.163	0.163	0.173	0.163	0.163
	SD	0.050	0.036	0.050	0.028	0.050	0.023	0.036	0.028	0.036	0.023
	P	0.240		0.052 *		0.156		0.174		0.915	

Given are mean $MTR_{Rex}APT$, $MTR_{Rex}MT$, $APTw_{asym}$ and MT_{const} values for methemoglobin (mHb), hemosiderin (Hs) and contrast-enhancing (CE_C) and whole tumor volumes (WT_C) corrected for mHb and Hs. The table further indicates the results from Mann–Whitney-U-tests testing for differences in mean CEST contrast values between mHb and Hs, mHb and CE_C/WT_C, as well as Hs and CE_C/WT_C. *p*-values ≤ 0.05 are indicated by an asterisk (*). The table quantifies the lower mean of $MTR_{Rex}APT$-, $MTR_{Rex}MT$- and MT_{const} values for mHb in comparison to corrected tumor volumes, which are visually demonstrated for an exemplary participant in Figure 2. Although very visible on Figure 3, the $MTR_{Rex}APT$ did not show higher mean values for Hs in comparison to corrected tumor volumes.

Table A2. Association of uncorrected and corrected tumor volumes with therapy response.

Tumor Volume		**CE**	**CE_C**	**WT**	**WT_C**
MTR_{Rex} APT	P	0.546	0.458	0.523	0.501
	AUC	0.438	0.424	0.566	0.569
	BP sens	0.500	0.500	0.688	0.688
	BP spez	0.556	0.556	0.556	0.556
MTR_{Rex} MT	P	0.081	0.044 *	0.184	0.208
	AUC	0.677	0.705	0.635	0.628
	BP sens	0.556	0.667	0.500	0.500
	BP spez	0.813	0.688	0.875	0.938
$APTw_{ASYM}$	P	0.904	0.986	0.717	0.617
	AUC	0.514	0.503	0.538	0.552
	BP sens	0.667	0.667	0.278	0.556
	BP spez	0.625	0.563	1.000	0.625
MT_{const}	P	0.001 *	0.002 *	<0.001 *	<0.001 *
	AUC	0.826	0.816	0.868	0.861
	BP sens	0.667	0.722	0.722	0.722
	BP spez	1.000	0.938	0.938	0.938
Participants (n)		34			

Given are the results of receiver operator characteristic (ROC) analyses and log rank tests testing for the associations of mean CEST contrast values of uncorrected and corrected tumor volumes with therapy response, as assessed according to response assessment in neuro-oncology (RANO) criteria. Given are *p*-values, areas under the curve (AUC) and best pairs (BP) for optimal sensitivity (sens.) and specificity (spec.) for uncorrected contrast-enhancing (CE) and whole tumor (WT) volumes, as well as contrast-enhancing (CE_C) and whole tumor volumes (WT_C) corrected for methemoglobin and hemosiderin. *p*-values ≤ 0.05 are indicated by an asterisk (*).

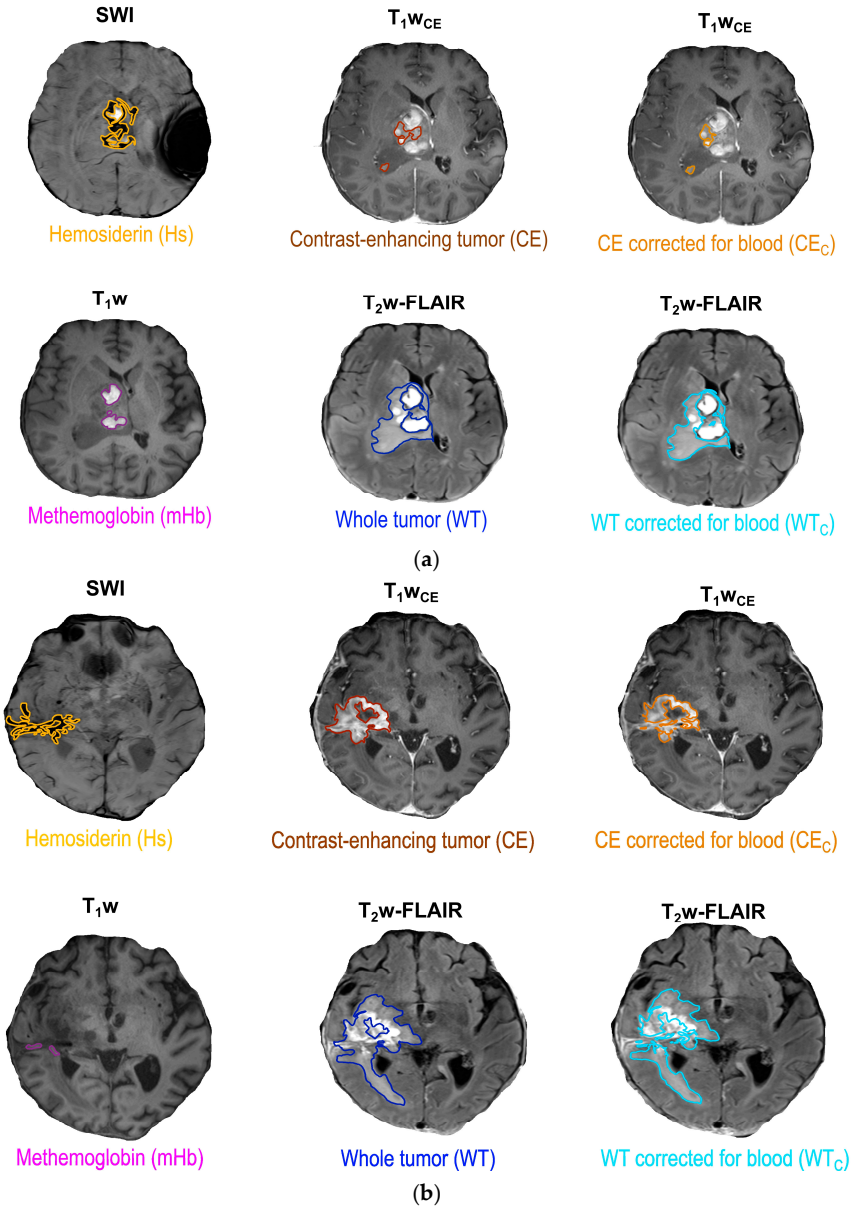

Figure A1. Segmentation of uncorrected and corrected tumor volumes. Displayed are representative ROIs of methemoglobin (mHb), hemosiderin (Hs), contrast-enhancing tumor (CE), corrected contrast-enhancing tumor (CE_C), whole tumor and corrected whole tumor (WT_C) in two representative participants with larger depositions of mHb (**a**) and Hs (**b**). Depicted are mHb on T_1w imaging, Hs on susceptibility-weighted imaging (SWI), contrast-enhancing tumor volumes without (CE) and with correction for mHb and Hs (CE_C) on contrast-enhanced T_1w (T_1w_{CE}) images, as well as whole tumor volumes (WT) without and with correction for mHb and Hs (WT_C) on T_2w-FLAIR images. WT encompassed contrast-enhancing tumor tissue and T_2w-FLAIR-hyperintense tissue changes. Larger mHb depositions that were identifiable as such due to localization in the resection cavity or larger surrounding Hs deposition with marked T_2w-FLAIR signal drop were grossly excluded for CE and WT. CE_C and WT_C were calculated from CE and WT in MATLAB® (Mathworks, version 2019b, MA, USA) by subtracting overlapping mHb and Hs. The figure illustrates how the investigated blood products and uncorrected tumor volumes were defined on T_1w, SWI, T_1w_{CE} and T_2w-FLAIR imaging in an exemplary participant with coexisting depositions of mHb and Hs and highlights the differences between uncorrected and corrected tumor volumes.

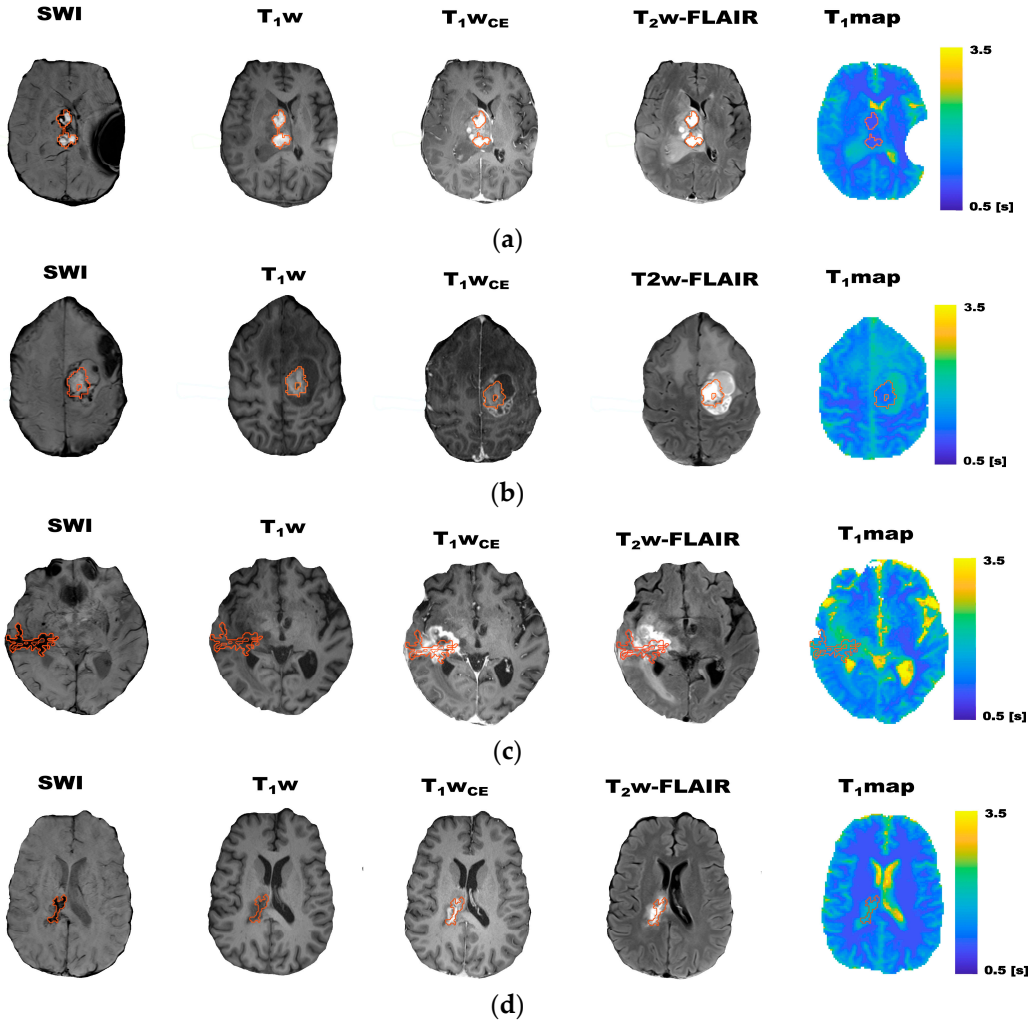

Figure A2. T1 maps of exemplary participants with larger methemoglobin and hemosiderin depositions. Displayed are the T1 maps for the four participants with larger methemoglobin (mHb; Subfigures (**a**,**b**)) and hemosiderin (Hs; (**c**,**d**)) depositions in the tumor area displayed in Figures 2 and 3. Given are T_2* susceptibility-weighted (SWI), T_1w, contrast-enhanced T_1w (T_1wCE) and T_2w-FLAIR images, as well as quantitative T_1 contrast maps. The ROIs indicate the T_1w-hyperintese mHb (**a**,**b**) and Hs (dark on SWI; (**c**,**d**)) on all contrast maps. mHb visually showed markedly decreased T_1 values. Hs visually showed diffusely elevated T_1 values (**d**). The figure highlights the T_1 contribution of mHb and Hs depositions, which especially affect MT_{const}, as well as $MTR_{Rex}APT$ and $MTR_{Rex}MT$ imaging.

Table A3. Association of mean CEST contrast values with survival for uncorrected and corrected tumor volumes.

Tumor Volume		CE	CE_C	WT	WT_C
$MTR_{Rex}APT$	P	0.056	0.110	0.417	0.417
	HR	2.439	2.110	1.526	1.525
	OS+	225	253	225	225
	OS−	416	392	392	392
$MTR_{Rex}MT$	P	0.919	0.964	0.559	0.847
	HR	0.958	1.068	1.389	1.179
	OS+	315	315	294	315
	OS−	280	280	280	225

Table A3. *Cont.*

Tumor Volume		CE	CE_C	WT	WT_C
$APTw_{asym}$	P	0.040 *	0.095	0.084	0.020 *
	HR	2.634	2.240	2.304	2.990
	OS+	215	215	225	215
	OS−	392	392	398	398
MT_{const}	P	0.068	0.068	0.044 *	0.044 *
	HR	2.330	2.330	2.536	2.536
	OS+	228	228	215	215
	OS−	315	315	392	392
Participants (n)		34			

The log rank test results for the association of mean CEST contrast values of uncorrected and corrected tumor volumes with survival. Given are the *p*-values, hazard ratios (HR) and the overall survival (in days) of participants with mean contrast values above (OS+) and below (OS-) the group medians for uncorrected contrast-enhancing (CE) and whole tumor (WT) volumes, as well as contrast-enhancing (CE_C) and whole tumor volumes (WT_C) corrected for methemoglobin and hemosiderin. *p*-values ≤ 0.05 are indicated by an asterisk (*).

References

1. Weller, M.; van den Bent, M.; Preusser, M.; Le Rhun, E.; Tonn, J.C.; Minniti, G.; Bendszus, M.; Balana, C.; Chinot, O.; Dirven, L.; et al. EANO guidelines on the diagnosis and treatment of diffuse gliomas of adulthood. *Nat. Rev. Clin. Oncol.* **2021**, *18*, 170–186. [CrossRef]
2. Zikou, A.; Sioka, C.; Alexiou, G.A.; Fotopoulos, A.; Voulgaris, S.; Argyropoulou, M.I. Radiation Necrosis, Pseudoprogression, Pseudoresponse, and Tumor Recurrence: Imaging Challenges for the Evaluation of Treated Gliomas. *Contrast Media Mol. Imaging* **2018**, *2018*, 6828396. [CrossRef] [PubMed]
3. Henriksen, O.M.; Álvarez-Torres, M.D.M.; Figueiredo, P.; Hangel, G.; Keil, V.C.; Nechifor, R.E.; Riemer, F.; Schmainda, K.M.; Warnert, E.A.H.; Wiegers, E.C.; et al. High-Grade Glioma Treatment Response Monitoring Biomarkers: A Position Statement on the Evidence Supporting the Use of Advanced MRI Techniques in the Clinic, and the Latest Bench-to-Bedside Developments. Part 1: Perfusion and Diffusion Techniques. *Front. Oncol.* **2022**, *12*, 810263. [CrossRef] [PubMed]
4. Booth, T.C.; Wiegers, E.C.; Warnert, E.A.H.; Schmainda, K.M.; Riemer, F.; Nechifor, R.E.; Keil, V.C.; Hangel, G.; Figueiredo, P.; Álvarez-Torres, M.D.M.; et al. High-Grade Glioma Treatment Response Monitoring Biomarkers: A Position Statement on the Evidence Supporting the Use of Advanced MRI Techniques in the Clinic, and the Latest Bench-to-Bedside Developments. Part 2: Spectroscopy, Chemical Exchange Saturation, Multiparametric Imaging, and Radiomics. *Front. Oncol.* **2021**, *11*, 811425.
5. van Zijl, P.C.M.; Lam, W.W.; Xu, J.; Knutsson, L.; Stanisz, G.J. Magnetization Transfer Contrast and Chemical Exchange Saturation Transfer MRI. Features and analysis of the field-dependent saturation spectrum. *NeuroImage* **2018**, *168*, 222–241.
6. Doeberitz, N.v.K.; Kroh, F.; Breitling, J.; König, L.; Maksimovic, S.; Graß, S.; Adeberg, S.; Scherer, M.; Unterberg, A.; Bendszus, M.; et al. CEST imaging of the APT and ssMT predict the overall survival of patients with glioma at the first follow-up after completion of radiotherapy at 3T. *Radiother. Oncol.* **2023**, *184*, 109694. [CrossRef]
7. Mehrabian, H.; Myrehaug, S.; Soliman, H.; Sahgal, A.; Stanisz, G.J. Evaluation of Glioblastoma Response to Therapy with Chemical Exchange Saturation Transfer. *Int. J. Radiat. Oncol. Biol. Phys.* **2018**, *101*, 713–723. [CrossRef] [PubMed]
8. Paech, D.; Dreher, C.; Regnery, S.; Meissner, J.-E.; Goerke, S.; Windschuh, J.; Oberhollenzer, J.; Schultheiss, M.; Deike-Hofmann, K.; Bickelhaupt, S.; et al. Relaxation-compensated amide proton transfer (APT) MRI signal intensity is associated with survival and progression in high-grade glioma patients. *Eur. Radiol.* **2019**, *29*, 4957–4967. [CrossRef] [PubMed]
9. Regnery, S.; Adeberg, S.; Dreher, C.; Oberhollenzer, J.; Meissner, J.-E.; Goerke, S.; Windschuh, J.; Deike-Hofmann, K.; Bickelhaupt, S.; Zaiss, M.; et al. Chemical exchange saturation transfer MRI serves as predictor of early progression in glioblastoma patients. *Oncotarget* **2018**, *9*, 28772–28783. [CrossRef]
10. Chan, R.W.; Chen, H.; Myrehaug, S.; Atenafu, E.G.; Stanisz, G.J.; Stewart, J.; Maralani, P.J.; Chan, A.K.M.; Daghighi, S.; Ruschin, M.; et al. Quantitative CEST and MT at 1.5T for monitoring treatment response in glioblastoma: Early and late tumor progression during chemoradiation. *J. Neurooncol.* **2021**, *151*, 267–278.
11. Kroh, F.; Doeberitz, N.V.K.; Breitling, J.; Maksimovic, S.; König, L.; Adeberg, S.; Scherer, M.; Unterberg, A.; Bendszus, M.; Wick, W.; et al. Semi-solid MT and APTw CEST-MRI predict clinical outcome of patients with glioma early after radiotherapy. *Magn. Reson. Med.* **2023**, *90*, 1569–1581. [CrossRef] [PubMed]
12. Meissner, J.; Korzowski, A.; Regnery, S.; Goerke, S.; Breitling, J.; Floca, R.O.; Debus, J.; Schlemmer, H.; Ladd, M.E.; Bachert, P.; et al. Early response assessment of glioma patients to definitive chemoradiotherapy using chemical exchange saturation transfer imaging at 7 T. *J. Magn. Reson. Imaging* **2019**, *50*, 1268–1277. [CrossRef]
13. Ma, B.; Blakeley, J.O.; Hong, X.; Zhang, H.; Jiang, S.; Blair, L.; Zhang, Y.; Heo, H.-Y.; Zhang, M.; van Zijl, P.C.M.; et al. Applying amide proton transfer-weighted MRI to distinguish pseudoprogression from true progression in malignant gliomas. *J. Magn. Reson. Imaging* **2016**, *44*, 456–462. [CrossRef] [PubMed]

14. Liu, J.; Li, C.; Chen, Y.; Lv, X.; Lv, Y.; Zhou, J.; Xi, S.; Dou, W.; Qian, L.; Zheng, H.; et al. Diagnostic performance of multiparametric MRI in the evaluation of treatment response in glioma patients at 3T. *J. Magn. Reson. Imaging* **2020**, *51*, 1154–1161. [CrossRef]
15. Park, J.E.; Kim, H.S.; Park, K.J.; Kim, S.J.; Kim, J.H.; Smith, S.A. Pre- and Posttreatment Glioma: Comparison of Amide Proton Transfer Imaging with MR Spectroscopy for Biomarkers of Tumor Proliferation. *Radiology* **2016**, *278*, 514–523. [CrossRef]
16. Park, K.J.; Kim, H.S.; Park, J.E.; Shim, W.H.; Kim, S.J.; Smith, S.A. Added value of amide proton transfer imaging to conventional and perfusion MR imaging for evaluating the treatment response of newly diagnosed glioblastoma. *Eur. Radiol.* **2016**, *26*, 4390–4403. [CrossRef]
17. Park, Y.W.; Ahn, S.S.; Kim, E.H.; Kang, S.-G.; Chang, J.H.; Kim, S.H.; Zhou, J.; Lee, S.-K. Differentiation of recurrent diffuse glioma from treatment-induced change using amide proton transfer imaging: Incremental value to diffusion and perfusion parameters. *Neuroradiology* **2021**, *63*, 363–372. [CrossRef]
18. Sanghvi, D. Post-treatment imaging of high-grade gliomas. *Indian J. Radiol. Imaging* **2015**, *25*, 102–108. [CrossRef] [PubMed]
19. Sawaya, R.; Ueda, J.; Saito, S. Quantitative Susceptibility Mapping and Amide Proton Transfer-Chemical Exchange Saturation Transfer for the Evaluation of Intracerebral Hemorrhage Model. *Int. J. Mol. Sci.* **2023**, *24*, 6627. [CrossRef]
20. Wang, M.; Hong, X.; Chang, C.-F.; Li, Q.; Ma, B.; Zhang, H.; Xiang, S.; Heo, H.-Y.; Zhang, Y.; Lee, D.-H.; et al. Simultaneous detection and separation of hyperacute intracerebral hemorrhage and cerebral ischemia using amide proton transfer MRI. *Magn. Reson. Med.* **2015**, *74*, 42–50.
21. Lai, J.H.; Liu, J.; Yang, T.; Huang, J.; Liu, Y.; Chen, Z.; Lee, Y.; Leung, G.K.; Chan, K.W. Chemical Exchange Saturation Transfer Magnetic Resonance Imaging for Longitudinal Assessment of Intracerebral Hemorrhage and Deferoxamine Treatment at 3T in a Mouse Model. *Stroke* **2023**, *54*, 255–264. [CrossRef]
22. Zaiss, M.; Windschuh, J.; Paech, D.; Meissner, J.-E.; Burth, S.; Schmitt, B.; Kickingereder, P.; Wiestler, B.; Wick, W.; Bendszus, M.; et al. Relaxation-compensated CEST-MRI of the human brain at 7T: Unbiased insight into NOE and amide signal changes in human glioblastoma. *NeuroImage* **2015**, *112*, 180–188. [CrossRef]
23. Zhou, J.; Zaiss, M.; Knutsson, L.; Sun, P.Z.; Ahn, S.S.; Aime, S.; Bachert, P.; Blakeley, J.O.; Cai, K.; Chappell, M.A.; et al. Review and consensus recommendations on clinical APT-weighted imaging approaches at 3T: Application to brain tumors. *Magn. Reson. Med.* **2022**, *88*, 546–574. [PubMed]
24. Zhou, J.; Heo, H.-Y.; Knutsson, L.; van Zijl, P.C.; Jiang, S. APT-weighted MRI: Techniques, current neuro applications, and challenging issues. *J. Magn. Reson. Imaging* **2019**, *50*, 347–364. [PubMed]
25. Goerke, S.; Soehngen, Y.; Deshmane, A.; Zaiss, M.; Breitling, J.; Boyd, P.S.; Herz, K.; Zimmermann, F.; Klika, K.D.; Schlemmer, H.P.; et al. Relaxation-compensated APT and rNOE CEST-MRI of human brain tumors at 3 T. *Magn. Reson. Med.* **2019**, *82*, 622–632. [CrossRef]
26. Wen, P.Y.; Chang, S.M.; Bent, M.J.V.D.; Vogelbaum, M.A.; Macdonald, D.R.; Lee, E.Q. Response assessment in neuro-oncology clinical trials. *J. Clin. Oncol.* **2017**, *35*, 2439. [CrossRef]
27. Louis, D.N.; Perry, A.; Wesseling, P.; Brat, D.J.; Cree, I.A.; Figarella-Branger, D.; Hawkins, C.; Ng, H.K.; Pfister, S.M.; Reifenberger, G.; et al. The 2021 WHO Classification of Tumors of the Central Nervous System: A summary. *Neuro-Oncology* **2021**, *23*, 1231–1251. [PubMed]
28. Eisenstat, D.D.; Pollack, I.F.; Demers, A.; Sapp, M.V.; Lambert, P.; Weisfeld-Adams, J.D.; Burger, P.C.; Gilles, F.; Davis, R.L.; Packer, R.; et al. Impact of tumor location and pathological discordance on survival of children with midline high-grade gliomas treated on Children's Cancer Group high-grade glioma study CCG-945. *J. Neurooncol.* **2015**, *121*, 573–581.
29. Deshmane, A.; Zaiss, M.; Lindig, T.; Herz, K.; Schuppert, M.; Gandhi, C.; Bender, B.; Ernemann, U.; Scheffler, K. 3D gradient echo snapshot CEST MRI with low power saturation for human studies at 3T. *Magn. Reason. Med.* **2019**, *81*, 2412–2423. [CrossRef]
30. Zaiss, M.; Ehses, P.; Scheffler, K. Snapshot-CEST: Optimizing spiral-centric-reordered gradient echo acquisition for fast and robust 3D CEST MRI at 9.4 T. *NMR Biomed.* **2018**, *31*, e3879. [CrossRef]
31. Schuenke, P.; Windschuh, J.; Roeloffs, V.; Ladd, M.E.; Bachert, P.; Zaiss, M. Simultaneous mapping of water shift and B1 (WASABI)-Application to field-Inhomogeneity correction of CEST MRI data. *Magn. Reson. Med.* **2017**, *77*, 571–580. [CrossRef]
32. Breitling, J.; Korzowski, A.; Kempa, N.; Boyd, P.S.; Paech, D.; Schlemmer, H.; Ladd, M.E.; Bachert, P.; Goerke, S. Motion correction for three-dimensional chemical exchange saturation transfer imaging without direct water saturation artifacts. *NMR Biomed.* **2022**, *35*, e4720. [CrossRef]
33. Windschuh, J.; Zaiss, M.; Meissner, J.-E.; Paech, D.; Radbruch, A.; Ladd, M.E.; Bachert, P. Correction of B1-inhomogeneities for relaxation-compensated CEST imaging at 7 T. *NMR Biomed.* **2015**, *28*, 529–537. [CrossRef] [PubMed]
34. Bradley, W.G., Jr. MR appearance of hemorrhage in the brain. *Radiology* **1993**, *189*, 15–26. [CrossRef] [PubMed]
35. Zheng, S.; van der Bom, I.M.J.; Zu, Z.; Lin, G.; Zhao, Y.; Gounis, M.J. Chemical exchange saturation transfer effect in blood. *Magn. Reson. Med.* **2014**, *71*, 1082–1092. [CrossRef]
36. Shah, S.M.; Mougin, O.E.; Carradus, A.J.; Geades, N.; Dury, R.; Morley, W.; Gowland, P.A. The z-spectrum from human blood at 7T. *NeuroImage* **2018**, *167*, 31–40. [CrossRef] [PubMed]